

**SYNTHESIS OF FACET-CONTROLLED PLATINUM
NANOCRYSTALS WITH ENHANCED ACTIVITIES TOWARD
OXYGEN REDUCTION**

A Dissertation
Presented to
The Academic Faculty

by

Chi-Ta Lee

In Partial Fulfillment
of the Requirements for the Degree
Master of Science in the
School of Chemical and Biomolecular Engineering

Georgia Institute of Technology
May 2018

COPYRIGHT © 2018 BY CHI-TA LEE

**SYNTHESIS OF FACET-CONTROLLED PLATINUM
NANOCRYSTALS WITH ENHANCED ACTIVITIES TOWARD
OXYGEN REDUCTION**

Approved by:

Dr. Younan Xia, Advisor
Department of Biomedical Engineering
Georgia Institute of Technology

Dr. Dennis W. Hess
School of Chemical and Biomolecular
Engineering
Georgia Institute of Technology

Dr. Seung Woo Lee
School of Mechanical Engineering
Georgia Institute of Technology

Date Approved: February 9, 2018

The thesis is dedicated to my parents, grandparents and sisters.

ACKNOWLEDGEMENTS

During my MS study, I've gotten a lot of academic and moral supports from various people. First of all, I would like to express my gratitude to my advisor, Professor Younan Xia, for the guidance and support in the past two years. He always provided insightful discussion that not only helps my research but also stimulates my critical thinking. I would like to extend my gratitude to Professors Dennis Hess and Seung Woo Lee for serving my committee. Thank you for all the advice and support for my work.

I greatly appreciate Dr. Hsin-Chieh Peng and Dr. Tung-Han Yang for helping me establish my knowledge in the research and sharing experience when I was new to Georgia Tech. I would like to thank Dr. Jinho Park, Dr. Xuan Yang, Dr. Ming Zhou, Dr. Helan Wang, Dr. Madeline Vara, Legna Figueroa-Cosme, Shan Zhou, Ming Zhao, Sujin Lee and many other current and former Xia group members for lots of help on my way to pursue my MS. I would like to make special thanks to Dr. Kyle D. Gilroy and Dr. Zachary D. Hood for tremendous help and discussion on my research.

My Sincerest thanks would go to my parents, Chi-Ming Lee and Tzu-Chiao Hung for their endless love, support. At last, I would like to thank all my friends in Taiwan for the continuous encouragement and support.

TABLE OF CONTENTS

ACKNOWLEDGEMENTS	iv
LIST OF TABLES	vi
LIST OF FIGURES	vii
LIST OF SYMBOLS AND ABBREVIATIONS	viii
SUMMARY	x
CHAPTER 1. Introduction	1
1.1 Platinum and Its Application	1
1.2 Strategies for Maximizing the Mass Activity of a Platinum Catalyst	3
2.1.1 Reduction of Particle Size	3
2.1.2 Control of Facet	4
1.3 Objectives	5
CHAPTER 2. Experimental Design	6
2.1 Synthesis of Platinum Nanocrystals	6
2.2 Characterizations	6
2.3 Preparation of Catalysts	7
2.4 Electrochemical Measurements	7
CHAPTER 3. Results and Discussion	9
2.1 Materials Synthesis and Characterization	9
2.2 Electrochemical Measurements	16
CHAPTER 4. Conclusions and Future Directions	21
2.1 Conclusions	21
2.2 Future Directions	22
REFERENCES	23

LIST OF TABLES

Table 4.1	Summary of the electrochemical data collected for the different catalysis.	20
-----------	--	----

LIST OF FIGURES

Figure 1.1	Schematic illustration showing the evolution from a precursor (in the center), through a homogeneous nucleation process to five types of seeds (in the middle ring) and then growth into nanocrystals with distinct shapes (in the outer ring).	2
Figure 3.1.1	(A) Schematic illustration and TEM images showing the Pt nanocrystals obtained using the standard protocol at (B) 18 h, (C) 24 h, and (D) 48 h, respectively.	10
Figure 3.1.2	TEM image of Pt octahedral nanocrystals obtained by extending the reaction time of a standard synthesis to 72 h.	11
Figure 3.1.3	TEM images of the Pt nanocrystals obtained using the standard protocol except for the variations of the other experimental parameters: (A, B) use of the reaction temperature at 80 °C and 100 °C, respectively; (C) with the addition of 13.4 μL of HCl and keeping the reaction at 100 °C; and (D) the introduction of ascorbic acid as an addition reducing agent.	12
Figure 3.1.4	TEM images of the Pt nanocrystals obtained using the standard protocol except for the variation in molar weight for the PVP used: (A) 10, (B) 40, and (C) 360 kDa.	15
Figure 3.1.5	(A) TEM, (B) low-magnification HAADF-STEM, and (C) atomic-resolution TEM images of the Pt octahedra synthesized using the standard protocol with a reaction time of 48 h. The inset in (A) and (B) show an octahedron oriented along one of its [100]-axes.	16
Figure 3.2.1	TEM image of 10-nm Pt cubes. Some of them were elongated bars, but their surfaces should all be largely covered by {100} facets. For simplicity, we refer all of them as “cube” in our discussion.	17
Figure 3.2.2	(A) cyclic voltammograms and (B) ORR polarization curves recorded from the Pt _{oct} /C, Pt _{cube} /C, and commercial Pt/C catalysts. The currents were normalized to the geometric area of the RDE (0.196 cm ²). (C) Mass and (D) specific activities given as kinetic currents (j_k) normalized to the Pt masses and the ECSAs of the catalysts, respectively. The color scheme in (A) applies to all other panels.	19

LIST OF SYMBOLS AND ABBREVIATIONS

AA	ascorbic acid
CV	cyclic voltammogram
CN	coordination number
DI	deionized
ECSA	electrochemical surface area
<i>fcc</i>	face-centered cubic
HAADF	high-angle annular dark-field
HClO ₄	perchloric acid
HRTEM	high-resolution transmission electron microscopy
ICP-MS	inductively-coupled
j_k	the kinetic current density
$j_{k,mass}$	the kinetic current density per mass of Pt, mass activity
$j_{k,specific}$	the kinetic current density per electrochemical surface area, specific activity
LSV	linear sweep voltammogram
Na ₂ PtCl ₆	sodium hexachloroplatinate
ORR	oxygen reduction reaction
PEMFC	proton-exchange membrane fuel cells
PVP	poly(vinyl pyrrolidone)
ODE	rotating disk electrode
RHE	reversible hydrogen electrode
STEM	scanning transmission electron microscopy
TEM	transmission electron microscopy

V_{RHE}

electric potentials vs reversible hydrogen electrode

SUMMARY

Platinum (Pt) nanocrystals have been applied to a wide variety of applications due to their excellent catalytic properties. However, due to its scarcity, the high price of Pt has been prohibiting many technologies from being used on an industrial scale, such as proton-exchange membrane fuel cells (PEMFCs). It is estimated that the loading of Pt as the electrocatalyst in PEMFCs should be reduced by at least four-fold relative to that of state-of-art commercial Pt/C to make it profitable to commercialize PEMFCs. Therefore, it is appealing to develop new types of Pt catalysts to replace the state-of-art Pt/C catalyst. The surface structure of Pt nanocrystals has found to be critical to their interaction with reactant molecule, which directly relates to their catalytic activities. The surface structure can be directly impacted by the sizes, facets and surface strains of nanocrystals. By tuning one of the factors, the catalytic activity or selectivity could be significantly changed to many structure-sensitive reactions due to the change of the electronic structure of surface atom. In this work, I successfully developed a facile, aqueous-phase synthesis of Pt octahedra with an edge length of *c.a.* 8 nm. The Pt octahedra showed a specific activity of 1.5 mA cm⁻², much greater than that of commercial Pt/C, which only has a specific activity of 0.38 mA cm⁻². However, the mass activities are similar, which was attributed to its relative large particle size. Therefore, the future work will focus on reducing the size down below 5 nm to achieve closer specific electrochemical surface area (ECSA) of commercial Pt/C.

CHAPTER 1. INTRODUCTION

1.1 Platinum and Its Application

Platinum nanocrystals have drawn considerable attention owing to their extensive use as catalysts in a wide variety of industrially important applications, including catalytic converters in automobiles [1], hydrogenation reactions for the manufacturing of chemicals and pharmaceuticals [2], and acceleration of the ORR in PEMFCs [3-7]. Despite the excellent catalytic properties of Pt, its extreme scarcity in the earth's crust has presented a major challenge for the commercialization of new technologies such as PEMFCs on an industrial scale [8]. To address this issue, major efforts have been directed toward the engineering of Pt nanocatalysts for the achievement of maximum mass activity [9-15]. In the past decades, noble-metal nanocrystals have been successfully synthesized with a large variety of structures, such as sphere, cube, cuboctahedron, octahedron, tetrahedron, rod, plate, and icosahedron or decahedron, among others, as shown in Figure 1.1 [16]. The successful synthesis of shape-controlled Pt nanocrystals has advanced the use of Pt in electrocatalysis and catalysis [17]. For structure-sensitive reactions, such as ORR, the catalytic performance of Pt nanocrystals is known to be sensitive to their surface structure [18], in addition to the size.

Heterogeneous catalysis refers to a chemical reaction where gas or liquid phase of reactants firstly adsorb on a solid phase catalyst, transform to products, and then desorb [19]. It was found that the activity of catalyst is strongly correlated to the adsorption energy between the catalytic surface and reactants or products, and the adsorption energy cannot be too large or too small to achieve the optimal activity for the catalysts [20]. The well-

known volcano plot was then obtained by plotting the catalytic activity as a function of the heat of adsorption, where the highest activity could be achieved with the moderate binding energy [21]. For the ORR, which takes place in the cathode of PEMFC, Pt presents excellent electrocatalytic activity for accelerating this sluggish reaction. The adsorption of oxygen species on the Pt (binding energy between Pt and oxygen species) is the key for this reaction. To achieve the moderate binding energy of Pt and oxygen species would be the strategy to optimize the electrocatalytic activity of Pt. In the next section, I introduce a series of strategies that could possibly enhance the activities of Pt catalysts for ORR.

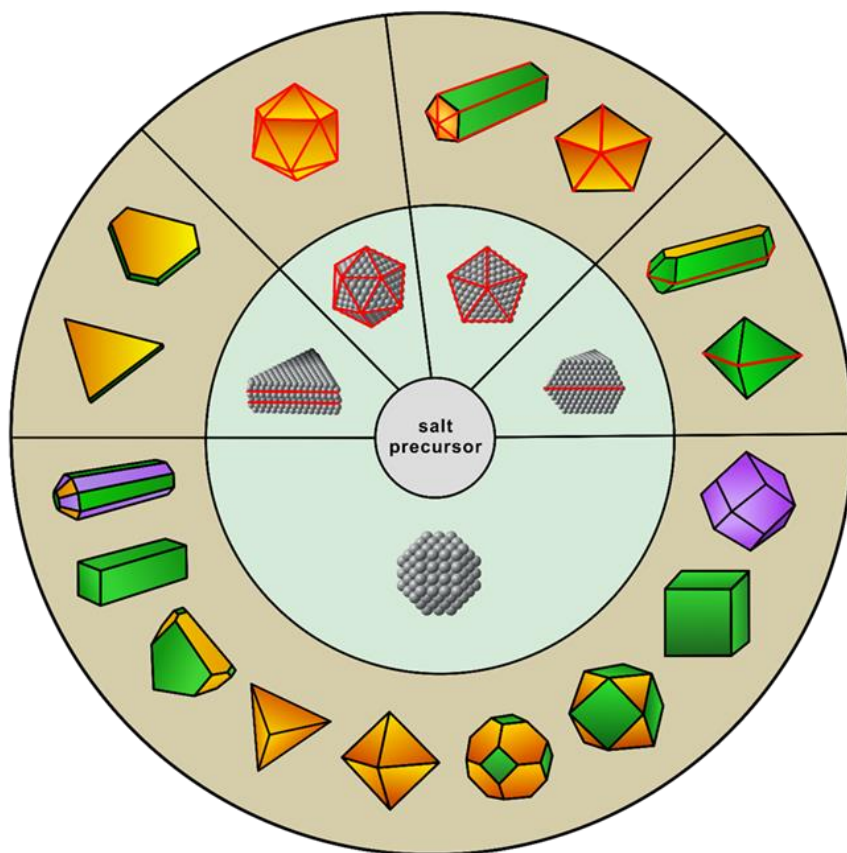


Figure 1.1. Schematic illustration showing the evolution from a precursor (in the center), through a homogeneous nucleation process to five types of seeds (in the middle ring) and then growth into nanocrystals with distinct shapes (in the outer ring). (Reprinted with permission from [16]. Copyright 2017 The Royal Society of Chemistry.)

1.2 Strategies for Maximizing the Mass Activity of a Platinum Catalyst

1.2.1 Reduction of Particle size

It is critical to cost down the Pt-based catalysts due to their high prices and scarcity. The most straightforward way is to reduce the size of Pt particles. In catalytic reaction, only the Pt atoms located on the surface takes part in the reaction. Therefore, the strategy to achieve higher surface-to-volume ratio is to reduce the size of Pt particles [22]. In current usage of nanoparticles in industrial catalysts, the sizes are usually in the range of 1-20 nm [23]. For examples, the commercial carbon supported platinum nanoparticles (Pt/C) used for PEMFCs is designed as 2-3 nm Pt spheres on carbon support, which provides high specific ECSA. However, there are still limited synthesis for the Pt nanocrystals with well-defined shapes under 10 nm.

In addition, the types of atoms on the surface are also influential to their catalytic activities. For a given nanocrystal, there are three types of atoms located at vertex, edge, and surface, which are distinguished by different coordination numbers (CNs) with adjacent atoms. In general, the CNs of different types of atoms are in an order of face > edge > vertex. The activity is very sensitive to the CNs of the surface atoms because of their different electronic structures which result in the different interaction between surface atom and reactants (binding energy) [24]. In essence, the proportion of various types of atoms is even more related to the size than the shape of a nanocrystal. The proportions of atoms on the vertex and edge will dramatically decrease with the size of a nanocrystal, and therefore the catalytic activity could change a lot with the same structure but different sizes. People believe that low CNs atoms on the surface of catalyst might present better activity;

nevertheless, in some other catalytic reactions, the high CNs atoms possess superior activity. Taking an example regarding Pt nanocrystals for ORR, Shoemaker and co-workers presented that the specific activity of Pt/C toward ORR could be enhanced with the increase of particle size in the range of 1-5 nm due to the decrease of edge sites (low CNs Pt atoms) [25]. However, the highest mass activity could only be achieved with the size of 2.2 nm. This is a good example showing that to achieve optimal mass activity requires a compromise between the utilization of Pt atoms and the proportion of various types of atoms on the surface.

1.2.2 Control of Facet

Both experimental and computational studies have demonstrated that the catalytic activity and selectivity of a metal nanocrystal are highly sensitive to shape [17,24,26]. The catalytic performance of metal nanocrystals in a given heterogeneous reaction has a strong correlation with the arrangement of atoms in the outermost layer. The facets expressed on a nanocrystal will determine the nature of the active sites and the energetics of a catalytic reaction. To this end, Somorjai and co-workers investigated the hydrogenation of benzene on cubic and cuboctahedral Pt nanocrystals [27,28]. They discovered that the reaction on Pt cubic nanocrystals enclosed by {100} facets only produced cyclohexane, whereas Pt cuboctahedral nanocrystals enclosed by a mix of {100} and {111} facets yielded a mixture of cyclohexane and cyclohexene. As for ORR, Marković and co-workers revealed that the electro-catalytic activity of Pt single-crystal substrates with different low-index facets increased in the order of Pt(100) \ll Pt(111) < Pt(110) in perchloric acid [18,29,30]. This

result clearly demonstrates that different types of facets on the Pt nanocrystals can yield significantly different catalytic activities.

1.3 Objectives

Although Pt nanocubes can be readily synthesized with the use of carbon monoxide as a capping agent toward the {100} facets [31,32], it has not been easy or straightforward to produce Pt octahedral nanocrystals. The most popular protocol reported in literature involves the mediation of Ag⁺ ions and thus the incorporation of Ag into the octahedral nanocrystals [33]. Progress was recently made by Huang and co-workers, who successfully synthesized pure Pt octahedra with an edge length of 30 nm at 160 °C with the use of oleylamine as a solvent [34]. However, in this case, the utilization efficiency of Pt atoms is quite low due to the relatively low surface-to-volume ratio associated with the large particle size. To be competitive with the commercial Pt/C catalyst, it is critical to reduce the size of the octahedral nanocrystals down to 5 nm. As other major drawbacks, the protocols reported in literature also need to use elevated reaction temperatures, dangerous and/or environmentally unfriendly reagents (*e.g.*, hydrogen gas [35,36] or organic solvents [30,37]), as well as multiple steps, such as seed-mediated growth [38] that requires several rounds of washing. In this work, we addressed these issues by developing a simple, one-step, low-temperature, and environmentally friendly method capable of generating sub-10 nm Pt octahedra. We also provide mechanistic insights along with catalytic measurements toward ORR.

CHAPTER 2. EXPERIMENTAL DESIGN

2.1 Synthesis of Platinum Nanocrystals

Materials. Sodium hexachloroplatinate (Na_2PtCl_6) was purchased from Alfa Aesar. Poly(vinyl pyrrolidone) (PVP, $M_w \approx 10,000, 40,000, 55,000$ and $360,000$), ascorbic acid (AA), oleylamine, oleic acid, tungsten hexacarbonyl were all obtained from Sigma–Aldrich and used as received. Platinum(II) acetylacetonate was bought from Acros Organics. Hydrochloric acid was purchased from Fisher Chemical. Deionized (DI) water with a resistivity of $18.2 \text{ M}\Omega \cdot \text{cm}$ at room temperature was used for all the experiments.

Preparation of sub-10-nm Pt octahedra and cubes: For a typical synthesis of Pt octahedra, we prepared 11 mL of an aqueous solution containing PVP (45.2 mg) and Na_2PtCl_6 (36.9 mg) in a 20 mL vial. The vial was then capped and maintained at $90 \text{ }^\circ\text{C}$ in an oil bath under magnetic stirring for 48 h. The final product was collected *via* centrifugation at 17500 rpm for 20 min, washed three times with water, and finally dispersed in water for further use. The Pt cubes were synthesized by following a protocol reported by Zou and co-workers [32].

2.2 Characterizations

TEM images were taken by using a Hitachi HT7700 microscope operated at 120 kV. The samples for TEM were prepared by drop casting the nanoparticle dispersions on carbon-coated Cu grids and drying under ambient conditions. High-resolution TEM (HRTEM) and high-angle annular dark-field scanning TEM (HAADF-STEM) were performed using an aberration-corrected Hitachi HD-2700 microscope operated at 200 kV.

The sample for HRTEM was washed with DI water, centrifuged 10 times, and dispersed in ethanol. A drop of the as-prepared solution was placed on a copper grid coated with a thin lacey carbon film. The metal contents were measured using inductively coupled plasma mass spectrometry (ICP-MS, NexION 300Q, Perkin Elmer).

2.3 Preparation of Catalysts

First, we loaded the Pt octahedra on the carbon support (Ketjen Black) at a loading amount of 15% by weight (as determined using ICP-MS). In order to clean the surface of the particles, the carbon-supported Pt octahedra were dispersed in 10 mL of acetic acid and then kept at 60 °C for 2 h. Afterwards, the catalyst was collected by centrifugation, and then washed with ethanol six times. After drying, 1 mg of the catalyst was dispersed in a mixture containing 0.8 mL of water, 0.2 mL of isopropanol, and 10 μ L of 5% Nafion under sonication for 1 h, producing the ink with a Pt concentration of 0.1242 mg mL⁻¹ (measured by ICP-MS). We then drop-casted 10 μ L of the ink onto a pre-cleaned glassy carbon rotating disk electrode (RDE, Pine Research Instrumentation) with a geometry area of 0.196 cm², and dried it at room temperature. Catalysts based on the Pt cubes and commercial Pt/C (20 wt% 3.2-nm Pt particles, Premetek Co.) were used for comparison. The inks of Pt_{cube}/C and Pt/C were prepared a protocol the same as what was used for the Pt octahedra. The ink was drop cast on the electrode with Pt loadings of 3.25 and 3.27 μ g for Pt_{cube}/C and Pt/C, respectively, as determined using ICP-MS.

2.4 Electrochemical Measurements

Electrochemical measurements were performed in a three-electrode system with a glassy carbon RDE (Pine Research Instrumentation), a Hydroflex hydrogen reference

electrode (Gaskatel) as the reference electrode, and a Pt coil as counter electrode connected to a CHI 600E potentiostat (CH Instruments). All potentials were converted to values in reference to the reversible hydrogen electrode (RHE). The electrolyte was 0.1 M HClO₄ solution prepared by diluting 70% stock solution with DI water. The CV curve was recorded in the potential range of 0.08-1.1 V_{RHE} with the scanning rate of 50 mV s⁻¹ in a nitrogen-saturated 0.1 M HClO₄ solution at room temperature. Then, we were able to calculate the specific ECSA of each catalyst by estimating the charges attributed to the desorption of hydrogen at the region of 0.08-0.5 V_{RHE} with reference values of 210 μC cm⁻² (for Pt_{cube}/C and commercial Pt/C) and 240 μC cm⁻² (for Pt_{oct}/C) for the desorption of a monolayer of hydrogen from Pt surfaces to get the ECSA, then dividing by the mass of Pt loaded on the working electrode. The ORR activities for the catalysts were measured in the same system with linear sweep voltammetry (LSV) except the 0.1 M HClO₄ electrolyte was saturated with oxygen and the working electrode was rotated at the rate of 1,600 rpm with a scanning rate of 10 mV s⁻¹. The kinetic current density (*j_k*) can be obtained from the Koutecky–Levich equation:

$$\frac{1}{j} = \frac{1}{j_k} + \frac{1}{j_d} \quad (1)$$

in which *j* is the measured current density and *j_d* is the diffusion-limiting current density. All the ORR data has been corrected by ohmic *iR* drop compensation and background currents.

CHAPTER 3. RESULTS AND DISCUSSION

3.1 Materials Synthesis and Characterization

To prepare the Pt octahedral nanocrystals, we simply mixed Na_2PtCl_6 and PVP in water and kept the aqueous solution at 90 °C for 48 hours. In this synthesis, the PVP can act as both a dispersing agent and a reducing agent. The hydroxyl end group contributes to the reducing capability to PVP [39]. Due to the mild reducing power of PVP, the color of the reaction solution remained light yellow up to 18 h into the synthesis. Afterwards, the color suddenly changed to transparent dark, indicating the formation of Pt nanoparticles, and then gradually darkened until becoming completely opaque. Since the reducing power of PVP is relatively weak as compared to other reducing agents traditionally used in colloidal nanocrystal syntheses, such as AA, the seeds can grow slowly into octahedra at a low concentration of free Pt(0) in the solution and additionally nucleation events are prevented from occurring.

Figure 3.1.1A shows a schematic illustration detailing the formation of Pt octahedra. In the early stage (up to 18 h), the reduction of Pt(IV) to Pt(0) contributed to the formation of Pt clusters that then evolved into seeds (*ca.* 3 nm in size), as shown by the transmission electron microscopy (TEM) image in Figure 3.1.1B. These initial seeds kept growing with the continuous supply of Pt(0) derived from the reduction of Pt(IV) precursor. At $t=24$ h, as shown by the TEM image in Figure 3.1.1C, the seeds had grown into truncated octahedra or octahedra of *ca.* 6 nm in edge length. When the reaction time was prolonged to 48 h, the

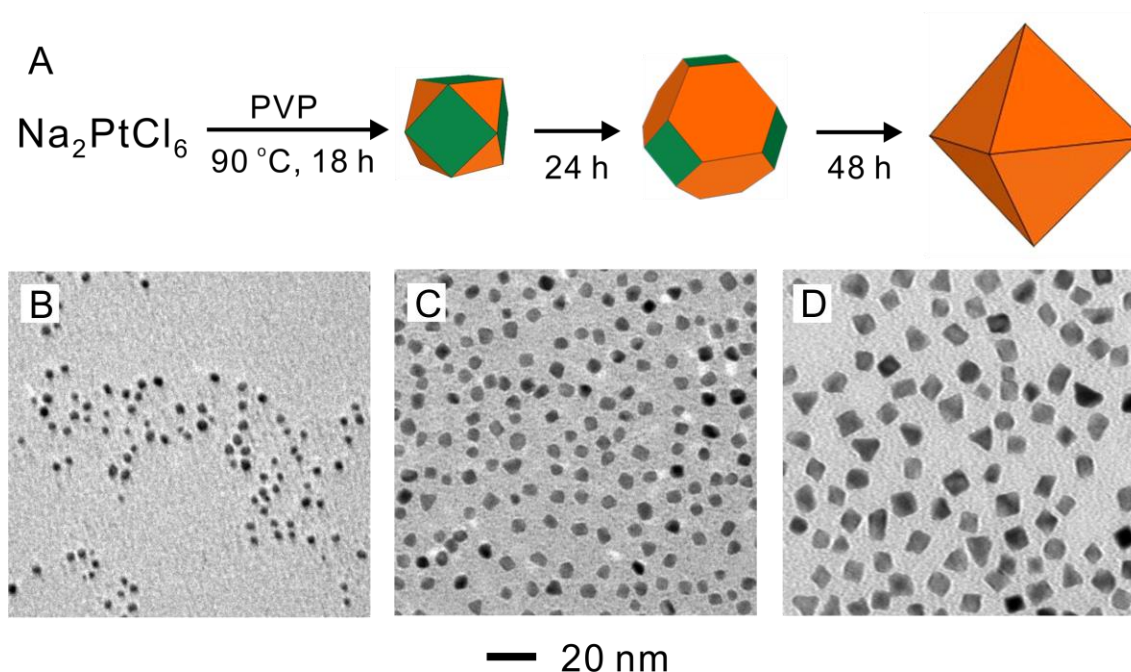


Figure 3.1.1. (A) Schematic illustration and TEM images showing the Pt nanocrystals obtained using the standard protocol at (B) 18 h, (C) 24 h, and (D) 48 h, respectively. (Reprinted with permission from [43]. Copyright 2017 John Wiley & Sons.)

truncated octahedra became octahedra of *ca.* 9 nm in edge length, as shown by the TEM image in Figure 3.1.1D. The preferential deposition of Pt atoms on the {100} facets of the seeds caused the particles to take an octahedral shape, together with a relatively uniform size. The size and shape of the octahedra showed no change when the reaction time was further extended to 72 h, as shown in Figure 3.1.2.

To explain the observed growth pattern, we argue that the growth is preferred along the $\langle 100 \rangle$ rather than $\langle 111 \rangle$ direction. It is possible that PVP binds more strongly to the {111} facets to give a higher packing density. However, no experimental or computational

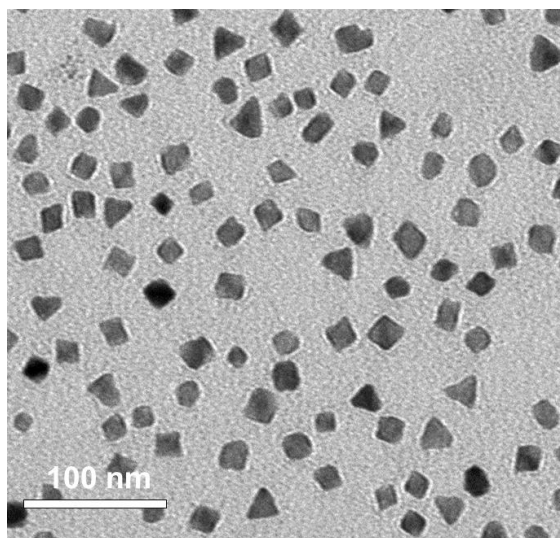


Figure 3.1.2. TEM image of Pt octahedral nanocrystals obtained by extending the reaction time of a standard synthesis to 72 h. (Reprinted with permission from [43]. Copyright 2017 John Wiley & Sons.)

evidence is available to support this assertion. On the other hand, from a kinetic point of view, there are two important factors that could contribute to the formation of octahedral nanocrystals enclosed by $\{111\}$ facets. Firstly, the deposition of Pt atoms should occur at a faster rate on $\{100\}$ facets as the specific surface free energy of the (100) surface is higher than that of the (111) surface and thereby has higher reactivity [40]. Secondly, if the surface diffusion of adatoms is substantial, the structure should trend away from octahedra and toward truncated octahedra because the latter structure has a relatively lower overall surface free energy. Therefore, it is instrumental to keep the reaction temperature sufficiently low to prevent the adatoms from migrating away from the initial deposition sites, promoting the formation of an octahedral structure.

To gain a deeper understanding of the atom deposition and nanocrystal growth processes, we further investigated the significance of reaction temperature on the morphology of the product. When the reaction temperature was lowered from 90 to 80 °C, while other experimental parameters were kept the same, we found that the side faces of the octahedral nanocrystals became somewhat concave, as shown in Figure 3.1.3A.

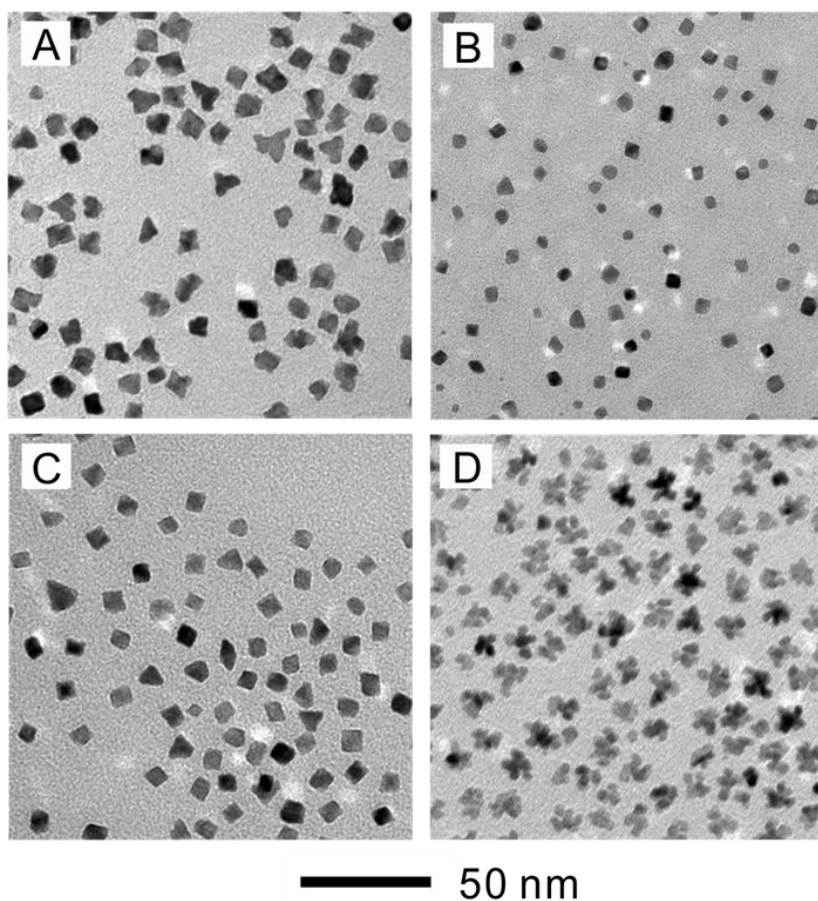


Figure 3.1.3. TEM images of the Pt nanocrystals obtained using the standard protocol except for the variations of the other experimental parameters: (A, B) use of the reaction temperature at 80 °C and 100 °C, respectively; (C) with the addition of 13.4 μL of HCl and keeping the reaction at 100 °C; and (D) the introduction of ascorbic acid as an addition reducing agent. (Reprinted with permission from [43]. Copyright 2017 John Wiley & Sons.)

This observation supports the aforementioned mechanism because slowing down the diffusion rate of adatoms should lead to an even greater piling up of Pt atoms at the initial deposition sites [41]. As a result, the Pt atoms were largely stacked at the {100} vertices of an octahedral nanocrystal. On the other hand, if we increased the reaction temperature to 100 °C, smaller octahedra (*ca.* 5 nm) were obtained, as shown in Figure 3.1.3B. In this case, the increase in temperature was conducive to a greater concentration of seeds in the reaction system. Consequently, there would be much less Pt(IV) precursor in the solution available for reduction and deposition on the Pt seeds, ultimately leading to the formation of smaller nanocrystals.

To further support the proposed growth mechanism, we devised an experimental system in which the temperature was fixed while the deposition rate could be controllably modulated. To this end, we slowed down the reaction by adding 13.4 μL aqueous HCl into a standard reaction solution while setting the temperature to 100 °C. Instead of forming the expected octahedra, we obtained much larger and more concave Pt octahedra (up to 12 nm), as shown in Figure 3.1.3C. This is the opposite of what we expected since decreasing the deposition rate while maintaining a high temperature should trend the structure toward the octahedral shape. To explain this behavior, we noticed that the final size of the particles was much greater as compared to the synthesis carried out at neutral pH. Such an increase in size could be attributed to the decrease in reduction rate for the Pt(IV) precursor at a low pH, and thus fewer seeds were involved. This gave rise to relatively larger particles, making it much more difficult for adatoms to effectively migrate away from the initial deposition sites (*i.e.*, the vertices) and across the large side faces. Unfortunately, we were unable to increase the surface diffusion rate by increasing the reaction temperature as limited by the

boiling point of water. To make this effect more dramatic, we further increased the reduction rate of the Pt(IV) precursor by introducing a relatively stronger reducing agent such as ascorbic acid. In this case, the color of the reaction solution turned dark after only 10 min, as opposed to the 18 h when PVP alone was used as the reducing agent. As evident from the TEM image in Figure 3.1.3D, using a stronger reducing agent gave rise to Pt nanodendrites, which can be attributed to the much faster deposition rate [42]. Overall, our results confirm that the success of generating octahedral nanocrystals rate in the absence of a possible capping agent toward the {111} facets require a relatively slow reduction.

The size of the Pt octahedral nanocrystals could also be readily controlled by varying the molar weight of PVP. As mentioned briefly before, thanks to the terminated hydroxyl group which possesses reducing capability, salt precursors can be reduced by PVP. In our experiment, we varied the molar weight of PVP while keeping its amount and all other reaction parameters the same. The TEM images in Figure 3.1.4 show that the particle size increased from 6 nm to 15 nm with the use of different molar weights of PVP ranging from 10 kDa to 360 kDa. The reducing power of PVP will decrease with increasing molecular weight or polymer chain length. When we used the PVP with a molar weight of 10 kDa, the solution started to turn dark after 12 h. On the other hand, the color did not change until $t=24$ h and it took a longer time to turn dark when 360 kDa PVP was used. In this case, a slower reduction rate resulted in the formation of fewer seeds and thus larger Pt octahedra in the final products. Overall, one can use both the temperature and molecular weight of PVP to manipulate the reduction rate and thus control the size of the Pt octahedral nanocrystals.

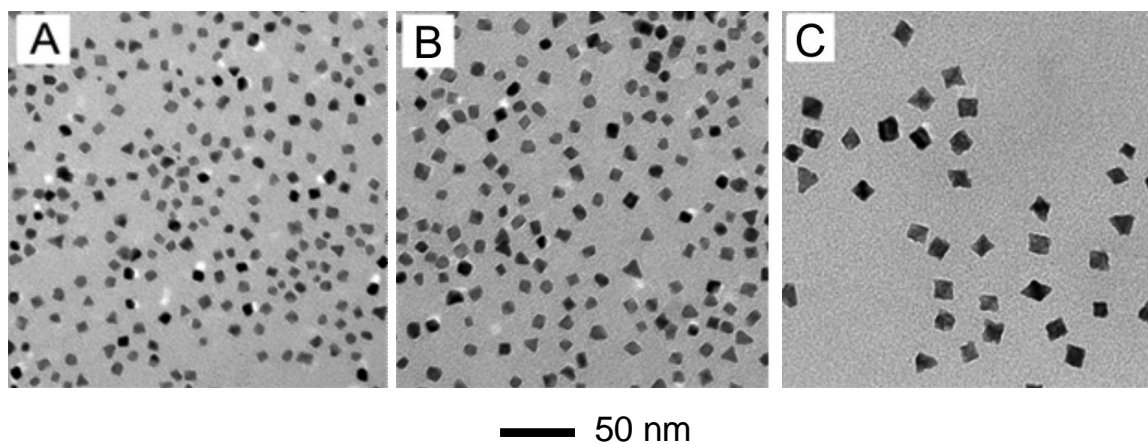


Figure 3.1.4. TEM images of the Pt nanocrystals obtained using the standard protocol except for the variation in molar weight for the PVP used: (A) 10, (B) 40, and (C) 360 kDa. (Reprinted with permission from [43]. Copyright 2017 John Wiley & Sons.)

Figure 3.1.5A shows a TEM image of Pt nanocrystals prepared using the standard protocol with a reaction time of 48 h. Among this relatively uniform sample, there were about 80% octahedra, 13% triangular plates, and 7% irregular particles. It is important to note that some of the octahedra may appear cubic under TEM because an octahedron can adopt a cubic profile when it is oriented along one of the $[100]$ -axes, as shown in the inset of Figure 3.1.5A. To confirm that the facets on these $[100]$ -oriented structures were indeed $\{111\}$, we captured both low-magnification HAADF-STEM and atomic-resolution TEM images, as shown in Figure 3.1.5B and Figure 3.1.5C. In the inset of Figure 3.1.5B, we are able to see the vertex of an octahedron on a square projection, which further confirmed that those with a square shape under conventional TEM are likely octahedra. From Figure 3.1.5C, we can clearly see the continuous and conformal extension of lattice in the same orientation, indicating that the octahedron is a single crystal. The image gives a lattice spacing of 0.23 nm, which is consistent with the $\{111\}$ lattice spacing of face-centered

cubic (fcc) Pt, confirming that the Pt octahedral nanocrystal is indeed enclosed by {111} facets.

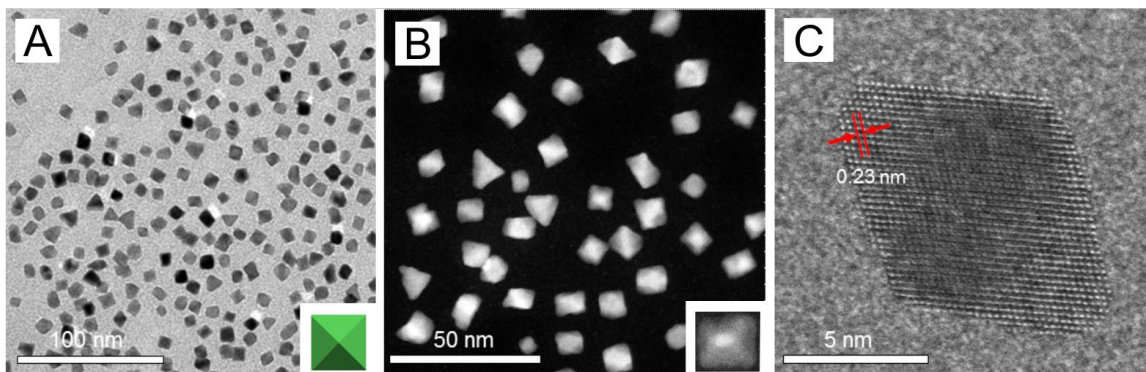


Figure 3.1.5. (A) TEM, (B) low-magnification HAADF-STEM, and (C) atomic-resolution TEM images of the Pt octahedra synthesized using the standard protocol with a reaction time of 48 h. The inset in (A) and (B) show an octahedron oriented along one of its [100]-axes. (Reprinted with permission from [43]. Copyright 2017 John Wiley & Sons.)

3.2 Electrochemical Measurement

We finally investigated the catalytic activity of Pt octahedra towards the ORR. In order to benchmark against structures enclosed by {100} facets, we also carried out electrochemical measurements on Pt nanocubes (edge length: 10 nm) shown in Figure 3.2.1, which were synthesized by following the protocol from the Fang group [28]. Before doing the measurement, we dispersed the Pt nanocrystals on carbon black in order to obtain Pt

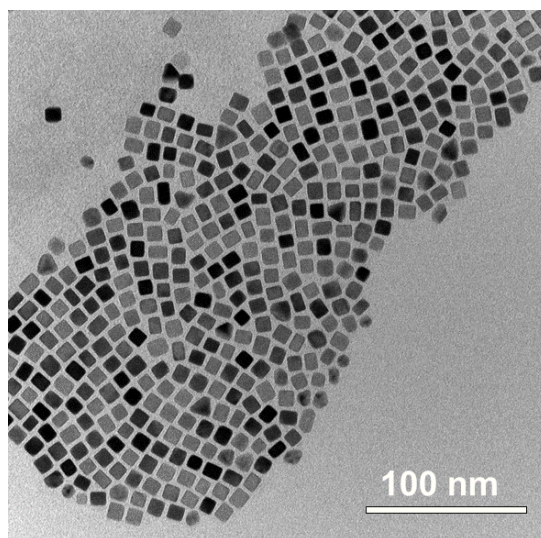


Figure 3.2.1. TEM image of 10-nm Pt cubes. Some of them were elongated bars, but their surfaces should all be largely covered by {100} facets. For simplicity, we refer all of them as “cube” in our discussion. (Reprinted with permission from [43]. Copyright 2017 John Wiley & Sons.)

octahedra/C ($\text{Pt}_{\text{oct}}/\text{C}$) and Pt cubes/C ($\text{Pt}_{\text{cube}}/\text{C}$) catalysts. Figure 3.2.2A shows cyclic voltammograms (CV) of these two different types of catalysts in the potential range of 0.08-1.1V. For the $\text{Pt}_{\text{cube}}/\text{C}$, there is a peak located on 0.3 V, which is attributed to hydrogen desorption on the {100} facets [18]. This peak does not show on the CV curve of $\text{Pt}_{\text{oct}}/\text{C}$, which confirms that almost no {100} facets exist. In order to calculate the electrochemical surface area (ECSA), we averaged the charges from the hydrogen adsorption and desorption peak, which were in the range of 0.08 and 0.5 V. As summarized in Table 1, the specific ECSAs of $\text{Pt}_{\text{oct}}/\text{C}$, $\text{Pt}_{\text{cube}}/\text{C}$, and commercial Pt/C were 16.80, 19.03, and 54.18 $\text{m}^2 \text{g}^{-1}$, respectively, which were calculated by normalizing by Pt mass on the electrode during measurements. The specific ECSAs of both octahedra and cubes were 3.2- and 2.8-fold less than that of Pt/C, respectively. The relatively large difference in the

specific ECSAs can be explained by the much smaller surface-to-volume ratio of the solid sub-10 nm octahedra and cubes.

Figure 3.2.2B shows the positive-going polarization curves by sweeping from 0.08 to 1.1 V. The specific and mass activities ($j_{k,\text{specific}}$ and $j_{k,\text{mass}}$) were calculated using the Koutecky–Levich equation and then normalized by the ECSA and Pt mass of the metal catalyst. In order to better understand the role played by faceting in the performance of catalyst (*i.e.*, {111} vs. {100} facets), we compared the mass and specific activities of Pt_{oct}/C and Pt_{cube}/C (Figure 3.2.2C and D). The specific activity of Pt octahedra is 1.5 mA cm⁻², which is about 5 times greater than that of Pt cubes (0.28 mA cm⁻²). This result was expected since many reports have demonstrated this trend [18,29,30]. However, even with such a high specific activity, the mass activity of Pt octahedra is only 0.25 A mg⁻¹, close to that of Pt/C (0.21 A mg⁻¹). This can be attributed to the relatively low ratio of the number of surface Pt atoms to the number of atoms in the bulk for our sub-10 nm octahedra. Therefore, many Pt atoms cannot participate in catalyzing ORR, leading to a low mass activity. Nevertheless, it is promising to significantly increase the mass activity by decreasing the size of the Pt octahedra. The Huang group has synthesized Pt octahedra of 30 nm in edge length but the size was too large to be used for the fuel cell industry [34]. In our case, we were able to remarkably reduce the size down to 10 nm in edge length, moving one step closer to the development of {111}-covered Pt catalysts for PEMFC applications.

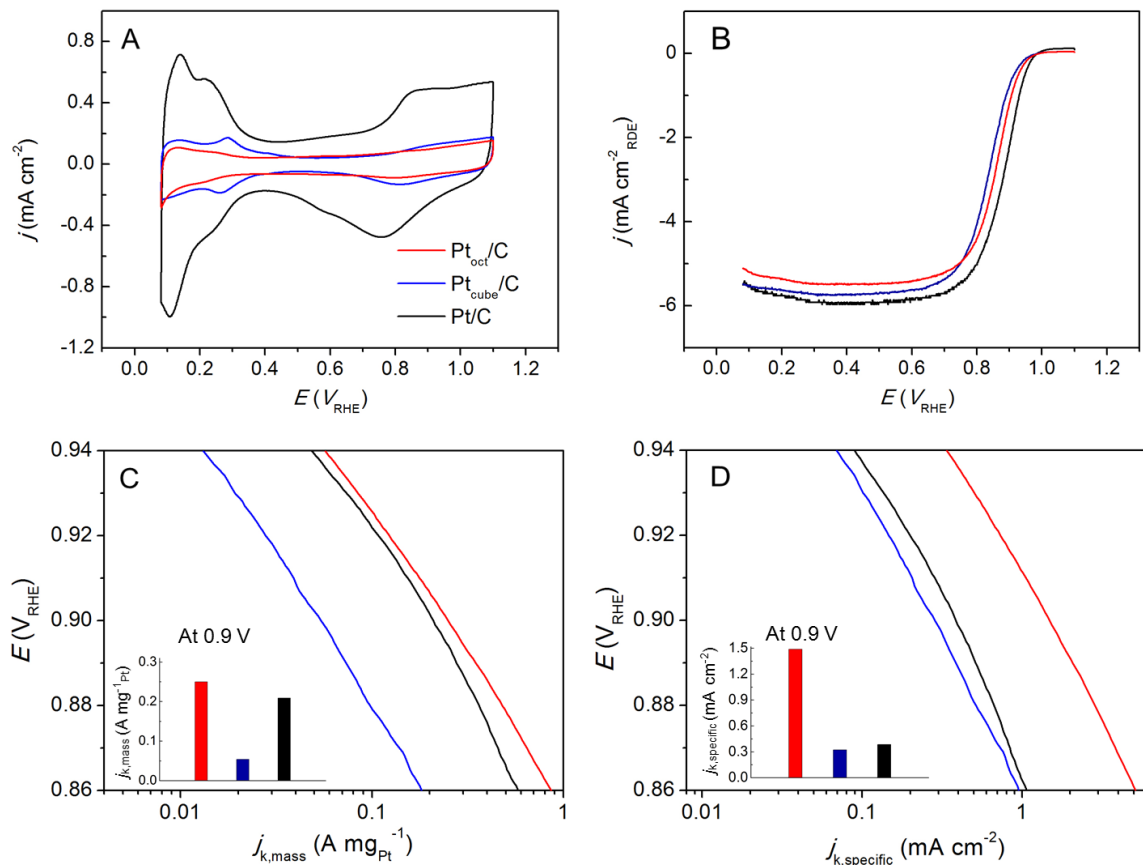


Figure 3.2.2. (A) cyclic voltammograms and (B) ORR polarization curves recorded from the Pt_{oct}/C, Pt_{cube}/C, and commercial Pt/C catalysts. The currents were normalized to the geometric area of the RDE (0.196 cm²). (C) Mass and (D) specific activities given as kinetic currents (j_k) normalized to the Pt masses and the ECSAs of the catalysts, respectively. The color scheme in (A) applies to all other panels. (Reprinted with permission from [43]. Copyright 2017 John Wiley & Sons.)

Table 3.2. Summary of the electrochemical data collected for the different catalysis. (Reprinted with permission from [43]. Copyright 2017 John Wiley & Sons.)

Catalyst	ECSA	SA at 0.9 V_{RHE}	MA at 0.9 V_{RHE}
	(m² g⁻¹Pt)	(mA cm⁻²)	(A mg⁻¹Pt)
Pt_{oct}/C	16.80	1.49	0.25
Pt_{cube}/C	19.03	0.28	0.05
Pt/C	54.18	0.385	0.21

CHAPTER 4. CONCLUSIONS AND FUTURE DIRECTIONS

4.1 Conclusions

In summary, we have successfully synthesized sub-10 nm Pt octahedra by reducing Na_2PtCl_6 with PVP in water. By conducting the reaction under slow reduction conditions over an extended period of time and at a proper temperature, Pt atoms were preferably deposited on the relative high surface energy {100}-facets, causing the nanocrystals to evolve into an octahedral shape. In addition, when surface diffusion of adatoms was decelerated by lowering the reaction temperature, a kinetically-controlled product (octahedra with concave side faces) was obtained. Moreover, we could manipulate the reduction rates by changing the reaction temperature or pH in generating Pt octahedra with different sizes. Most significantly, the specific activity of the Pt octahedra was found to be five- and four-times greater than those of Pt nanocubes and commercial Pt/C, respectively. It should be pointed out that this is the first time that sub-10 nm Pt octahedra could be synthesized in a colloidal synthesis. Taken together, this work promises a simple way toward the production of Pt octahedral nanocrystals with optimal size and activity for PEMFC application.

4.2 Future Directions

The Pt octahedra are promising for use as an ORR catalyst for PEMFCs. However, the particle size in the preliminary study is too large for any real application. By estimation, the Pt octahedra with a size of 4 nm in edge length can achieve a specific ECSA comparable to that of commercial Pt/C, and the mass activity can thereby be significantly enhanced by at least 4-fold relative to that of commercial Pt/C. Therefore, the proposed work is to further reduce the particle size down to 5 nm and below. According to the results from the preliminary study, I can manipulate the particle size by adjusting the reduction kinetics. Therefore, I decide to vary the kinetic parameters by altering experimental conditions such as the types/concentrations of reagents, temperature, and additives, instead of thermodynamic parameters (*e.g.*, surface capping).

REFERENCES

1. G. C. Koltsakis, A. M. Stamatelos, *Prog. Energy Combust. Sci.* **1997**, *23*, 1-39.
2. F. Roessler, *Chimia* **1996**, *50*, 106-109.
3. B. C. H. Steele, A. Heinzl, *Nature* **2001**, *414*, 345-352.
4. H. A. Gasteiger, S. S. Kocha, B. Sompalli, F. T. Wagner, *Appl. Catal., B* **2005**, *56*, 9-35.
5. M. L. Perry, T. F. Fuller, *J. Electrochem. Soc.* **2002**, *149*, 59-67.
6. W. Vielstich, A. Lamm, H. A. Gasteiger, *Handbook of Fuel Cells-Fundamentals, Technology and Applications*, John Wiley & Sons, Chichester, **2003**.
7. M. Shao, *Electrocatalysis in Fuel Cells: A Non- and Low-Platinum Approach*, Springer, London, **2013**.
8. A. Rabis, P. Rodriguez, T. J. Schmidt, *ACS catal.* **2012**, *2*, 864-890.
9. J. Park, H. Wang, M. Vara, Y. Xia, *ChemSusChem* **2016**, *9*, 2855-2861.
10. J. Park, L. Zhang, S.-I. Choi, L. T. Roling, N. Lu, J. A. Herron, S. Xie, J. Wang, M. J. Kim, M. Mavrikakis, Y. Xia, *ACS Nano* **2015**, *9*, 2635-2647.
11. L. Zhang, L. T. Roling, X. Wang, M. Vara, M. Chi, J. Liu, S.-I. Choi, J. Park, J. A. Herron, Z. Xie, M. Mavrikakis, Y. Xia, *Science* **2015**, *349*, 412-416.
12. S. Xie, S.-I. Choi, N. Lu, L. T. Roling, J. A. Herron, L. Zhang, J. Park, J. Wang, M. J. Kim, Z. Xie, M. Mavrikakis, Y. Xia, *Nano Lett.* **2014**, *14*, 3570-3576.
13. S. R. Lee, J. Park, K. D. Gilroy, X. Yang, L. Figueroa-Cosme, Y. Ding, Y. Xia, *ChemCatChem* **2016**, *8*, 3082-3088.

14. X. Wang, L. Figueroa-Cosme, X. Yang, M. Luo, J. Liu, Z. Xie, Y. Xia, *Nano Lett.* **2016**, *16*, 1467-1471.
15. X. Wang, S.-I. Choi, L. T. Roling, M. Luo, C. Ma, L. Zhang, M. Chi, J. Liu, Z. Xie, J. A. Herron, M. Mavrikakis, Y. Xia, *Nat. Commun.* **2015**, *6*, 7594.
16. T.-H. Yang, K. D. Gilroy, Y. Xia, *Chem. Sci.* **2017**, in press.
17. J. Chen, B. Lim, E. P. Lee, Y. Xia, *Nano Today* **2009**, *4*, 81-95.
18. V. R. Stamenkovic, B. Fowler, B. S. Mun, G. Wang, P. N. Ross, C. A. Lucas, N. M. Marković, *Science* **2007**, *315*, 493-497.
19. M. E. Davis, R. J. Davis, *Fundamentals of Chemical Reaction Engineering*, McGraw-Hill: New York, **2003**.
20. P. Sabatier, *Ber. Dtsch. Chem. Ges.* **1911**, *44*, 1984.
21. A. A. Balandin, *Adv. Catal.* **1969**, *19*, 1.
22. Y. Xia, Y. Xiong, B. Lim, S. E. Skrabalak, *Angew. Chem. Int. Ed.* **2009**, *48*, 60-103.
23. I. Bertini, *Inorganic and Bio-inorganic Chemistry*, Eolss Publishers Co. Ltd., Oxford, United Kingdom, **2009**.
24. S. Xie, S.-I. Choi, X. Xia, Y. Xia, *Curr. Opin. Chem. Eng.* **2013**, *2*, 142-150.
25. M. Shao, A. Peles, K. Shoemaker, *Nano Lett.* **2011**, *11*, 3714-3719.
26. A. Ruditskiy, H.-C. Peng, Y. Xia, *Annu. Rev. Chem. Biomol. Eng.* **2016**, *7*, 327-348.
27. K. R. McCrea, G. A. Somorjai, *J. Mol. Catal. A: Chem.* **2000**, *163*, 43-53.
28. K. M. Bratlie, H. Lee, K. Komvopoulos, P. Yang, G. A. Somorjai, *Nano Lett.* **2007**, *7*, 3097-3101.

29. N.M. Marković, R.R. Adžić, B.D. Cahan, E.B. Yeager, *J. Electroanal. Chem.* **1994**, 377, 249-259.
30. N.M. Marković, P. N. Ross Jr., *Surf. Sci. Rep.* **2002**, 45, 117-229.
31. Y. Kang, X. Ye, C. B. Murray, *Angew. Chem. Int. Ed.* **2010**, 49, 6156-6159.
32. J. Zhang, H. Yang, J. Fang, S. Zou, *Nano Lett.* **2010**, 10, 638-644.
33. H. Song, F. Kim, S. Connor, G. A. Somorjai, P. Yang, *J. Phys. Chem. B* **2005**, 109, 188-193.
34. L. Bu, Y. Feng, J. Yao, S. Guo, J. Guo, X. Huang, *Nano Res.* **2016**, 9, 2811-2821.
35. Z. Peng, C. Kisielowski, A. T. Bell, *Chem. Commun.* **2012**, 48, 1854-1856.
36. H. Lee, S. E. Habas, S. Kweskin, D. Butcher, G. A. Somorjai, P. Yang, *Angew. Chem.* **2006**, 118, 7988-7992.
37. X. Huang, Z. Zhao, Y. Chen, E. Zhu, M. Li, X. Duan, Y. Huang, *Energy Environ. Sci.* **2014**, 7, 2957-2962.
38. Y. Xia, K. D. Gilroy, H.-C. Peng, X. Xia, *Angew. Chem. Int. Ed.* **2017**, 56, 60-95.
39. K. M. Koczkur, S. Mourdikoudis, L. Polavarapu, S. E. Skrabalak, *Dalton Trans.* **2015**, 44, 17883-17905.
40. Y. Xia, X. Xia, H.-C. Peng, *J. Am. Chem. Soc.* **2015**, 137, 7947-7966.
41. X. Xia, S. Xie, M. Liu, H.-C. Peng, N. Lu, J. Wang, M. J. Kim, Y. Xia, *Proc. Natl. Acad. Sci. U. S. A.* **2013**, 110, 6669-6673.
42. B. Lim, M. Jiang, P. H. C. Camargo, E. C. Cho, J. Tao, X. Lu, Y. Zhu, Y. Xia, *Science* **2009**, 324, 1302-1305.
43. C.-T Lee, X. Yang, M. Vara, K. D. Gilroy, Y. Xia, *ChemNanoMat* **2017**, 3, 879-884.